Published OnlineFirst January 8, 2015; DOI: 10.1158/2159-8290.CD-14-0736

RESEARCH ARTICLE

JAK–STAT Pathway Activation in Malignant and Nonmalignant Cells Contributes to MPN Pathogenesis and Therapeutic Response

Maria Kleppe[1], Minsuk Kwak[2], Priya Koppikar[1], Markus Riester[3,4], Matthew Keller[1], Lennart Bastian[1], Todd Hricik[1], Neha Bhagwat[1,5], Anna Sophia McKenney[1,5,6], Efthymia Papalexi[1], Omar Abdel-Wahab[1,7], Raajit Rampal[1,7], Sachie Marubayashi[1], Jonathan J. Chen[2], Vincent Romanet[8], Jordan S. Fridman[9], Jacqueline Bromberg[10], Julie Teruya-Feldstein[11], Masato Murakami[8], Thomas Radimerski[8], Franziska Michor[3,4], Rong Fan[2,12], and Ross L. Levine[1,7]

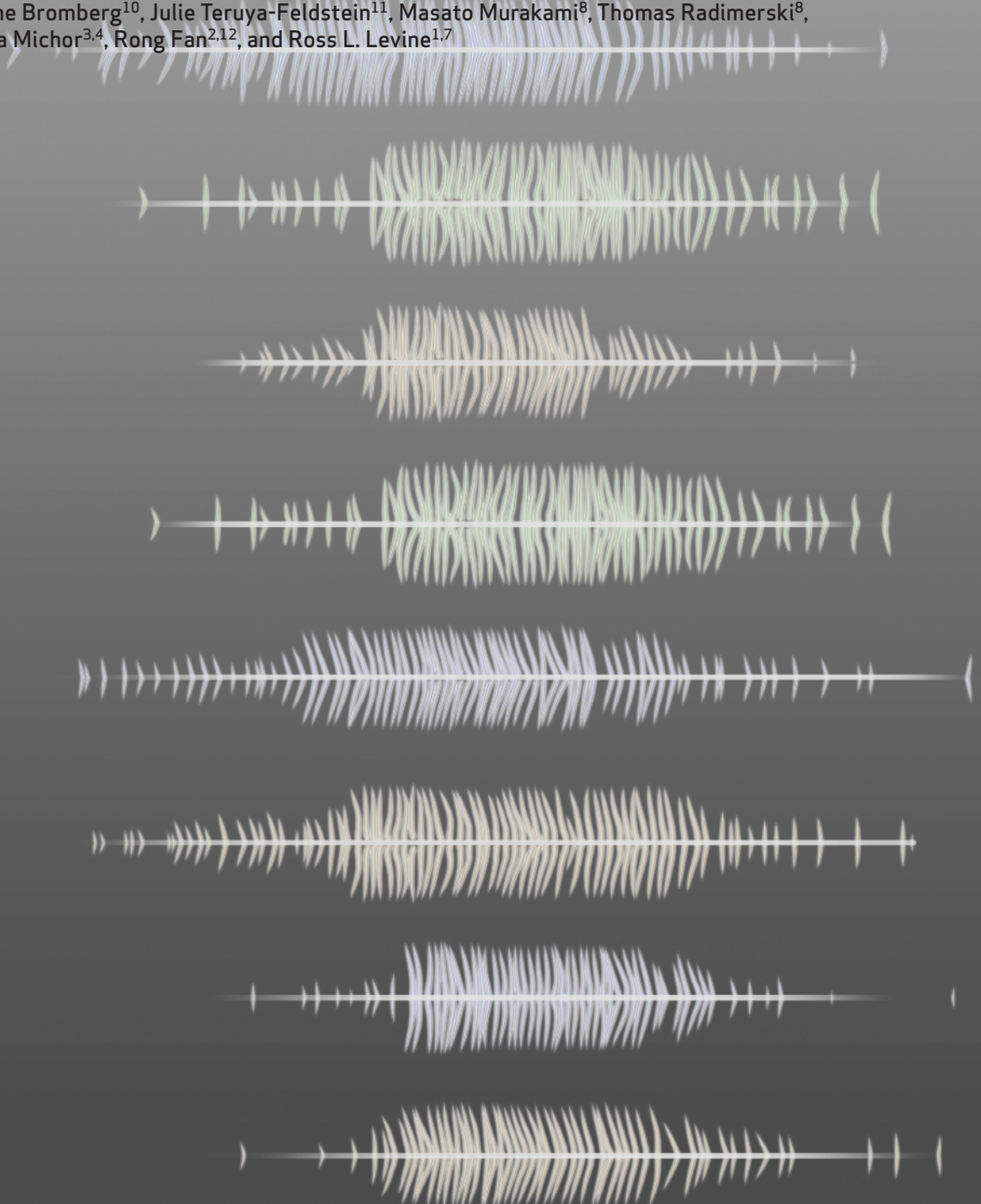

Published OnlineFirst January 8, 2015; DOI: 10.1158/2159-8290.CD-14-0736

ABSTRACT The identification of *JAK2/MPL* mutations in patients with myeloproliferative neoplasms (MPN) has led to the clinical development of JAK kinase inhibitors, including ruxolitinib. Ruxolitinib reduces splenomegaly and systemic symptoms in myelofibrosis and improves overall survival; however, the mechanism by which JAK inhibitors achieve efficacy has not been delineated. Patients with MPN present with increased levels of circulating proinflammatory cytokines, which are mitigated by JAK inhibitor therapy. We sought to elucidate mechanisms by which JAK inhibitors attenuate cytokine-mediated pathophysiology. Single-cell profiling demonstrated that hematopoietic cells from myelofibrosis models and patient samples aberrantly secrete inflammatory cytokines. Pan-hematopoietic *Stat3* deletion reduced disease severity and attenuated cytokine secretion, with similar efficacy as observed with ruxolitinib therapy. In contrast, *Stat3* deletion restricted to MPN cells did not reduce disease severity or cytokine production. Consistent with these observations, we found that malignant and nonmalignant cells aberrantly secrete cytokines and JAK inhibition reduces cytokine production from both populations.

SIGNIFICANCE: Our results demonstrate that JAK–STAT3-mediated cytokine production from malignant and nonmalignant cells contributes to MPN pathogenesis and that JAK inhibition in both populations is required for therapeutic efficacy. These findings provide novel insight into the mechanisms by which JAK kinase inhibition achieves therapeutic efficacy in MPNs. *Cancer Discov; 5(3); 316–31. ©2015 AACR.*

See related commentary by Belver and Ferrando, p. 234.

INTRODUCTION

Myeloproliferative neoplasms (MPN) are clonal hematopoietic disorders characterized by the proliferation of one or more myeloid lineages (1). Patients with MPN develop progressive splenomegaly, thrombosis, bleeding, and/or infection. Patients with MPN are also at cumulative risk to develop progressive bone marrow failure and/or transform to acute myeloid leukemia (AML), conditions which are associated with dismal clinical outcome (2). The discovery of cytokine-independent colony formation of MPN progenitors suggested that constitutive cytokine signaling contributes to MPN pathogenesis (3). The observation of somatic activating *JAK2*^{V617F} mutations in patients with polycythemia vera (PV), essential thrombocythemia (ET), and primary myelofibrosis (PMF) provided the first insight into the molecular basis of MPN (4–7). Subsequent studies identified somatic JAK–STAT pathway mutations in *JAK2*^{V617F}-negative MPN, most commonly in the *CALR* gene (8, 9) and the thrombopoietin receptor (*MPL*^{W515L}; ref. 10). These data underscore the central importance of genetic alterations in the JAK–STAT signaling pathway in MPN pathogenesis.

The discovery of *JAK2/MPL* mutations in the majority of patients with MPN provided the rationale for the clinical development of JAK kinase inhibitors for patients with MPN and subsequently for other malignancies. Clinical studies with JAK kinase inhibitors have shown that these agents improve splenomegaly, systemic symptoms, and overall survival (11). On the basis of these data, ruxolitinib, a JAK1/JAK2 kinase inhibitor, was approved for patients with myelofibrosis, and several other JAK inhibitors are in late-phase clinical trials. Although JAK inhibitors offer substantial clinical benefit to patients with MPN, the mechanisms by which these agents achieve clinical efficacy have not been fully delineated. Patients with MPN have significantly elevated circulating levels of proinflammatory cytokines, and increased circulating cytokine levels are associated with adverse survival in myelofibrosis (12). It has been hypothesized that the cytokine-driven inflammatory state in MPN contributes to the constitutional symptoms, bone marrow fibrosis, extramedullary hematopoiesis, and disease progression characteristic of these myeloid malignancies. JAK inhibitor therapy with ruxolitinib is associated with a reduction in the level of proinflammatory cytokines (13); however, the role of aberrant cytokine production in

[1]Human Oncology and Pathogenesis Program, Memorial Sloan Kettering Cancer Center, New York, New York. [2]Department of Biomedical Engineering, Yale University, New Haven, Connecticut. [3]Department of Biostatistics and Computational Biology, Dana-Farber Cancer Institute, Boston, Massachusetts. [4]Department of Biostatistics, Harvard School of Public Health, Boston, Massachusetts. [5]Gerstner Sloan Kettering Graduate School of Biomedical Sciences, New York, New York. [6]Weill Cornell/Rockefeller/Sloan Kettering Tri-Institutional MD–PhD Program, New York, New York. [7]Leukemia Service, Department of Medicine, Memorial Sloan Kettering Cancer Center, New York, New York. [8]Disease Area Oncology, Novartis Institutes for BioMedical Research, Basel, Switzerland. [9]Incyte Corporation, Wilmington, Delaware. [10]Breast Cancer Service, Department of Medicine, Memorial Sloan Kettering Cancer Center, New York, New York. [11]Department of Pathology, Memorial Sloan Kettering Cancer Center, New York, New York. [12]Yale Comprehensive Cancer Center, New Haven, Connecticut.

Note: Supplementary data for this article are available at Cancer Discovery Online (http://cancerdiscovery.aacrjournals.org/).

M. Kleppe and M. Kwak contributed equally to this article.

Corresponding Authors: Ross L. Levine, Human Oncology and Pathogenesis Program, Leukemia Service, Department of Medicine, Memorial Sloan Kettering Cancer Center, 415 East 68th Street, 1275 York Avenue, Box 20, New York, NY 10065. Phone: 646-888-2796; Fax: 646-422-0856; E-mail: leviner@mskcc.org; and Rong Fan, Department of Biomedical Engineering, 55 Prospect Street, New Haven, CT 06520. E-mail: rong.fan@yale.edu

doi: 10.1158/2159-8290.CD-14-0736

Published OnlineFirst January 8, 2015; DOI: 10.1158/2159-8290.CD-14-0736

myelofibrosis pathogenesis and in the response to JAK inhibitors remains to be delineated. We therefore sought to elucidate the role of aberrant cytokine production in MPN pathogenesis and in the response to JAK kinase inhibitors. We used a novel microfluidic single-cell profiling technique to examine the cytokine secretion profiles of myelofibrosis cells on a single-cell level and show that a significantly greater degree of multifunctionality and heterogeneity in cytokine production is a characteristic feature of myelofibrosis cells. Moreover, we show that JAK–STAT signaling in nonmutant hematopoietic cells contributes to MPN pathogenesis and that inhibition of JAK–STAT signaling in both mutant and nonmutant cells is required to reduce inflammatory signaling and to achieve clinical benefit in MPNs.

RESULTS

Proinflammatory Cytokines Are Elevated in Myelofibrosis Mice and Reversed with JAK1/2 Inhibitor Treatment

To identify cytokines that are altered in myelofibrosis, we measured the serum levels of 32 cytokines in the MPL^{W515L} bone marrow transplant myelofibrosis model (14) using multiplex bead-based Luminex technology. We identified a set of inflammatory cytokines, including IL6, CXCL9, and CCL2, which are elevated in the serum of MPL^{W515L}-mutant diseased mice (Fig. 1A), similar to the alterations in circulating cytokines observed in patients with myelofibrosis (12, 13). Ruxolitinib treatment (90 mg/kg, twice a day) normalized cytokine levels, consistent with the effects seen with chronic JAK inhibition in patients with MPN (Fig. 1A and Supplementary Fig. S1; ref. 13). Circulating cytokine levels were also elevated in myelofibrotic (6-month-old) *Jak2*^{V617F}*;Vav-Cre* knockin mice (Fig. 1B; ref. 15), and ruxolitinib treatment (60 mg/kg, twice a day) normalized cytokine levels in mice transplanted with *Jak2*^{V617F}-mutant cells (Fig. 1C). Short-term ruxolitinib treatment (3 doses, 90 mg/kg, twice a day) reduced cytokine production to a similar extent to that observed with 14 days of ruxolitinib treatment (90 mg/kg, twice a day; Fig. 1D), consistent with the rapid improvements in symptoms and splenomegaly seen with JAK inhibitor therapy (13) and with a direct effect of JAK kinase inhibition on cytokine secretion. The majority of cytokines (7 of 8) were also increased in the bone marrow supernatant (Fig. 1E) of MPL^{W515L}-mutant diseased

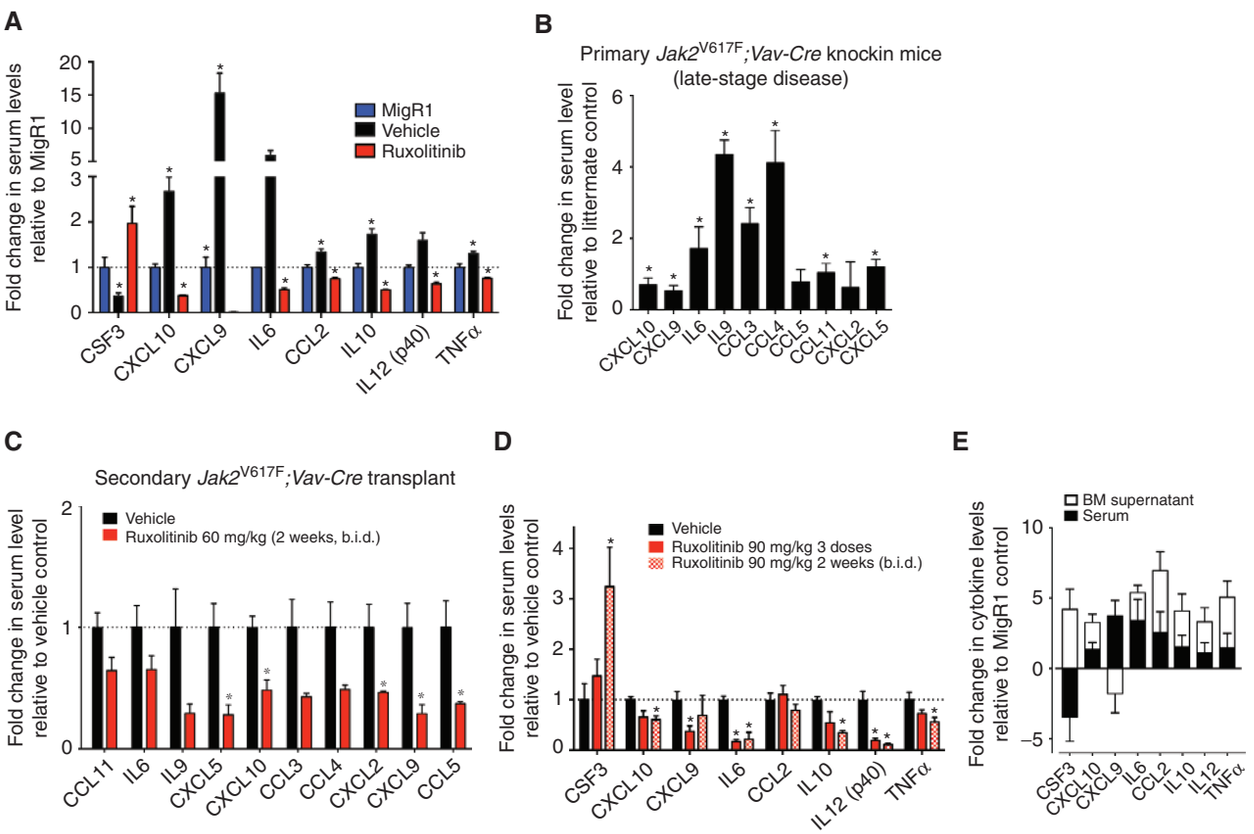

Figure 1. Proinflammatory cytokines are elevated in myelofibrosis mice and normalized with JAK inhibition. **A,** changes in cytokine levels in vehicle- and ruxolitinib-treated MPL^{W515L}-mutant mice compared with MigR1 mice. $n = 6$. *, $P < 0.05$. **B,** ruxolitinib [90 mg/kg, twice a day (b.i.d.)] reduces cytokines in mice transplanted with *Jak2*^{V617F}*;Vav-Cre*$^{+}$ cells. $n = 4$. *, $P < 0.05$. **C,** $\log_2$ fold changes in serum cytokine levels in primary JAK2^{V617F} knockin mice (late-stage disease) compared with age-matched littermate controls are shown. Mean ± SEM, $n = 9$ in each group. **D,** short-term treatment (3 doses, 90 mg/kg, twice a day) with ruxolitinib efficiently reduces serum cytokine levels in MPL^{W515L}-mutant diseased mice. $\log_2$ fold changes are displayed. $n = 4$. *, $P < 0.05$. **E,** $\log_2$ fold changes in serum and bone marrow (BM) supernatant in MPL^{W515L} mice compared with MigR1 mice. Mean ± SEM.

Published OnlineFirst January 8, 2015; DOI: 10.1158/2159-8290.CD-14-0736

mice, suggesting that aberrant cytokine production in myelofibrosis is, at least in part, derived from bone marrow cells.

Bone Marrow Myelofibrosis Cells Feature Aberrant Cytokine Secretion Profiles

To evaluate whether bone marrow cells are the source of aberrant cytokine production in myelofibrosis, we optimized a microchip system that allowed us to perform multiplexed measurements of up to 15 secretory cytokines from primary murine and human bone marrow cells at single-cell resolution (Fig. 2A; refs. 16–18). Hierarchical cluster analysis of the single-cell secretomic profiles delineated multiple distinct populations that displayed heterogeneous secretion signatures and revealed marked differences between myelofibrosis and control bone marrow cells (Fig. 2A). We observed a significant increase in the fraction of cytokine-secreting cells and in the extent of cytokine secretion per single myelofibrosis cell (Fig. 2B). These data suggest the increased cytokine production in myelofibrosis results from increased per-cell cytokine secretion and from an increase in the fraction of cytokine-secreting cells (Fig. 2C). The proportion of cells secreting at least one cytokine was significantly higher in myelofibrosis mice compared with control mice (67.6% vs. 46.6%; $P < 0.001$; Fisher exact test). The majority of cytokine-secreting control bone marrow cells (73%) secreted less than two cytokines, consistent with physiologic secretion of one cytokine per cell. In contrast, we found that bone marrow cells from myelofibrosis mice were composed of a significantly elevated frequency of multifunctional cells that cosecrete multiple cytokines: 43.9% of cells from myelofibrosis mice secreted two or more cytokines and 15.6% of cells secreted four or more cytokines compared with 1.2% in control mice (Fig. 2D).

To determine which cytokines were most frequently cosecreted by myelofibrosis cells, we calculated a mutual exclusivity *P* value for each pair of secreted cytokines (Fig. 2E). CCL3, CCL4, and TNFα were commonly cosecreted in myelofibrosis cells, and secretion of these cytokines was inversely correlated with the secretion of other cytokines (Fig. 2F). We observed cosecretion of all other cytokine combinations (IL6, IL12, IL10, CCL2, CCL5, CXCL9, and CXCL1) in myelofibrosis cells, consistent with the presence of at least two distinct populations of cytokine-secreting cells in myelofibrosis. In line with these observations, principal component analysis (PCA) demonstrated that a large proportion of normal bone marrow cells did not secrete any protein and other smaller subsets with distinct secretion patterns produced only one or two cytokines, most notably, CCL3 and CCL4 (Fig. 2G and Supplementary Fig. S2). In contrast, PCA maps of myelofibrosis bone marrow cells showed multiple, large populations with heterogeneous secretion signatures. We then used the Simpson diversity index to quantify the extent of heterogeneity in cytokine secretion, and found that this index increased significantly from 0.68 in normal cells to 0.85 in myelofibrosis cells ($P < 0.001$), consistent with a marked increase in the heterogeneity of single-cell cytokine secretion in myelofibrosis.

Mature Myeloid and Progenitor Cells Contribute to Aberrant Cytokine Levels *In Vivo*

We next sought to define which hematopoietic compartments contribute to aberrant cytokine secretion in myelofibrosis. We used the single-cell platform to profile mature myeloid cells (CD11b/Gr1 double-positive) and megakaryocyte/erythroid progenitor (MEP) cells from myelofibrosis and control mice. Similar to unfractionated bone marrow cells, GFP-positive myelofibrosis myeloid cells and MEP cells had an increase in the fraction of cytokine-secreting cells and increased cytokine secretion per cell (Supplementary Fig. S3). PCA analysis showed that each population had distinct cytokine secretion profiles (Fig. 3A). IL6 and IL10 were mainly secreted by MEPs, and mature myeloid cells were the main source of TNFα and CCL3 (Fig. 3B and Supplementary Fig. S3). These data indicate that different cell types have distinct cytokine secretion profiles and potentially distinct roles in myelofibrosis pathogenesis.

Aberrant Single-Cell Cytokine Secretion in PMF Cells

We next performed single-cell profiling of circulating granulocytes from patients with myelofibrosis and healthy individuals (Supplementary Table S1). The average secretion level of different cytokines was significantly elevated in myelofibrosis cells, resulting from both an increase in the fraction of cells secreting specific cytokines and the secretion level of individual cytokines per cell (Fig. 3C and D). Six out of eight cytokines (IL6, IL10, IL12, TNFα, CCL2, and CCL5), which were aberrantly secreted in our murine myelofibrosis model, were also secreted at a much higher level by PMF patient cells. We observed that IL8 was most highly secreted by myelofibrosis granulocytes; previous studies have shown that increased serum IL8 levels are associated with adverse outcome in myelofibrosis (12). Immunohistochemical analysis confirmed increased IL8 expression in myelofibrosis bone marrow sections, whereas control bone marrow cells showed only weak expression of IL8 (Supplementary Fig. S4). The proportion of cells secreting at least one cytokine was significantly increased in human myelofibrosis cells compared with control cells (41.4% vs. 14.6%; $P < 0.001$; Fisher exact test; Fig. 3E), demonstrating similar patterns of cytokine secretion in patients with myelofibrosis and murine models. Altogether, our single-cell profiling studies highlight the striking heterogeneity and multifunctionality in cytokine secretion profile in myelofibrosis.

Deletion of *Il6* from the Mouse System Shows Only Minor Effects on *Mpl*^{W515L}-Driven Disease

Previous studies of cytokine signaling in cancer have largely focused on IL6 as a mediator of inflammation in leukemia and other malignancies (19). Given that we found a significant increase in IL6 secretion in both MPN models and myelofibrosis patient cells, we first investigated the effects of *Il6* deletion on MPL^{W515L}-induced myelofibrosis *in vivo*. We assessed the specific role of IL6 in myelofibrosis *in vivo* by transplanting IL6-deficient myelofibrosis cells into IL6-deficient recipients. *Il6* deletion led to a modest reduction in white blood cell (WBC) count, but did not reduce spleen weight or the extent of myeloproliferation *in vivo* (Supplementary Fig. S5A and S5B). No significant differences were observed in the proportion of CD11b/Gr1 double-positive cells in the target organs (Supplementary Fig. S5C and S5D). Consistent with these data, we found that the serum levels of other proinflammatory

Published OnlineFirst January 8, 2015; DOI: 10.1158/2159-8290.CD-14-0736

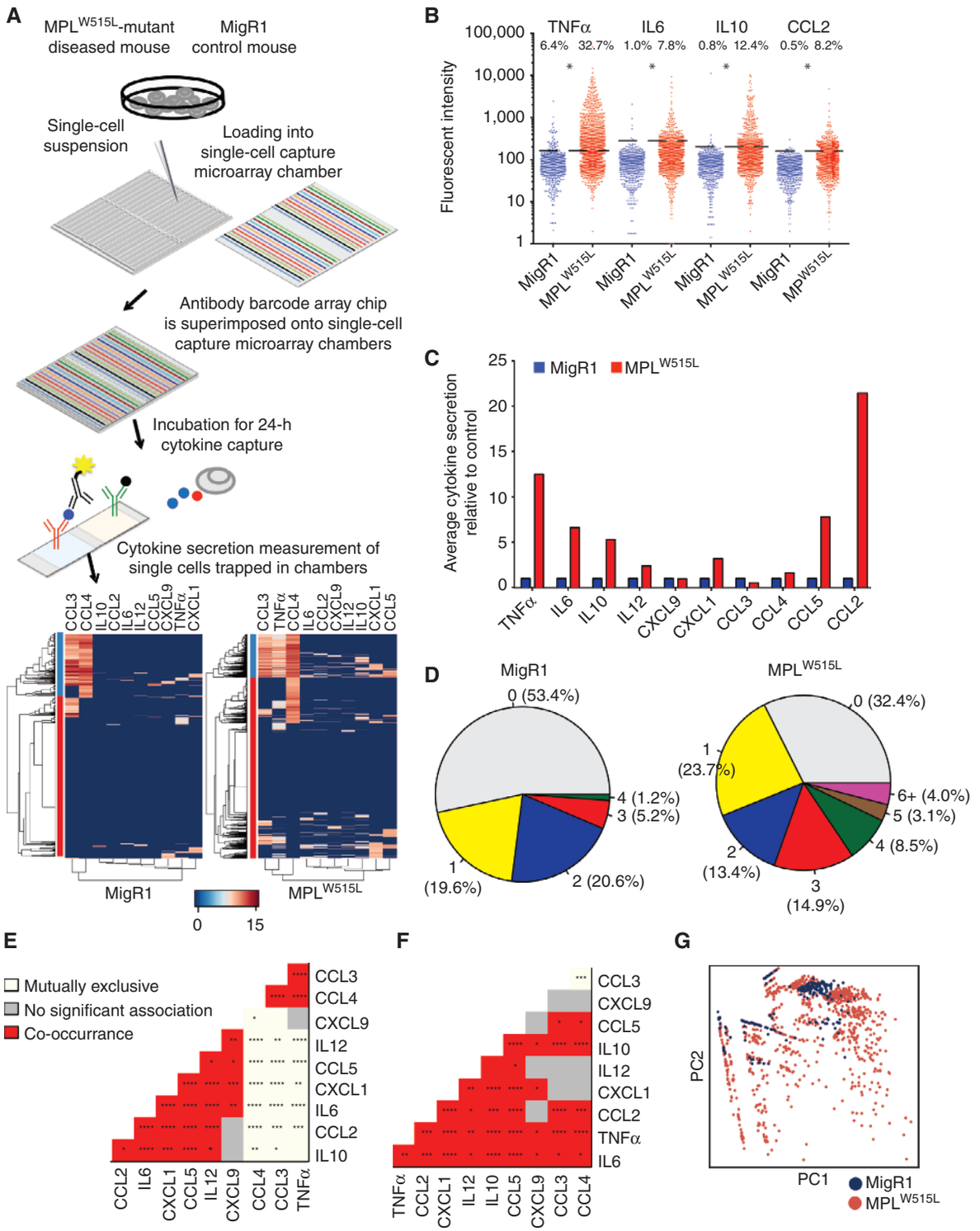

Figure 2. Bone marrow cells are potent cytokine producers. **A,** schematic display of single-cell cytokine secretion analysis workflow and hierarchical clustering of single-cell data from MPL^{W515L} and MigR1 whole bone marrow. Log_2-transformed values were used for cluster analysis. **B,** normalized fluorescent intensity for different cytokines. Numbers on top show cytokine secretion frequency. Dotted lines indicate cytokine secretion threshold. *, $P < 0.05$. **C,** total secretion levels (cytokine secretion fraction x average secretion intensity of cytokine secreting cells) of MPL^{W515L} mice bone marrow (MPL^{W515L}) relative to healthy control mice (MigR1) are shown. **D,** pie charts depicting proportion of MigR1 and MPL^{W515L} bone marrow cells secreting different numbers of cytokines (0–10). **E,** mutual exclusivity analysis for myelofibrosis cells. FDR: + < 0.05, ++ < 0.01 +++ < 0.001 and ++++ < 0.0001. Red/white without pluses is FDR < 0.1. **F,** comparison between cosecretion patterns observed in myelofibrosis and control cells. Colors visualize FDR. **G,** PCA of MPL^{W515L} and MigR1 cytokine secretion. MPL^{W515L}: $n = 2{,}254$ cells; MigR1 cells: $n = 608$ cells.

Published OnlineFirst January 8, 2015; DOI: 10.1158/2159-8290.CD-14-0736

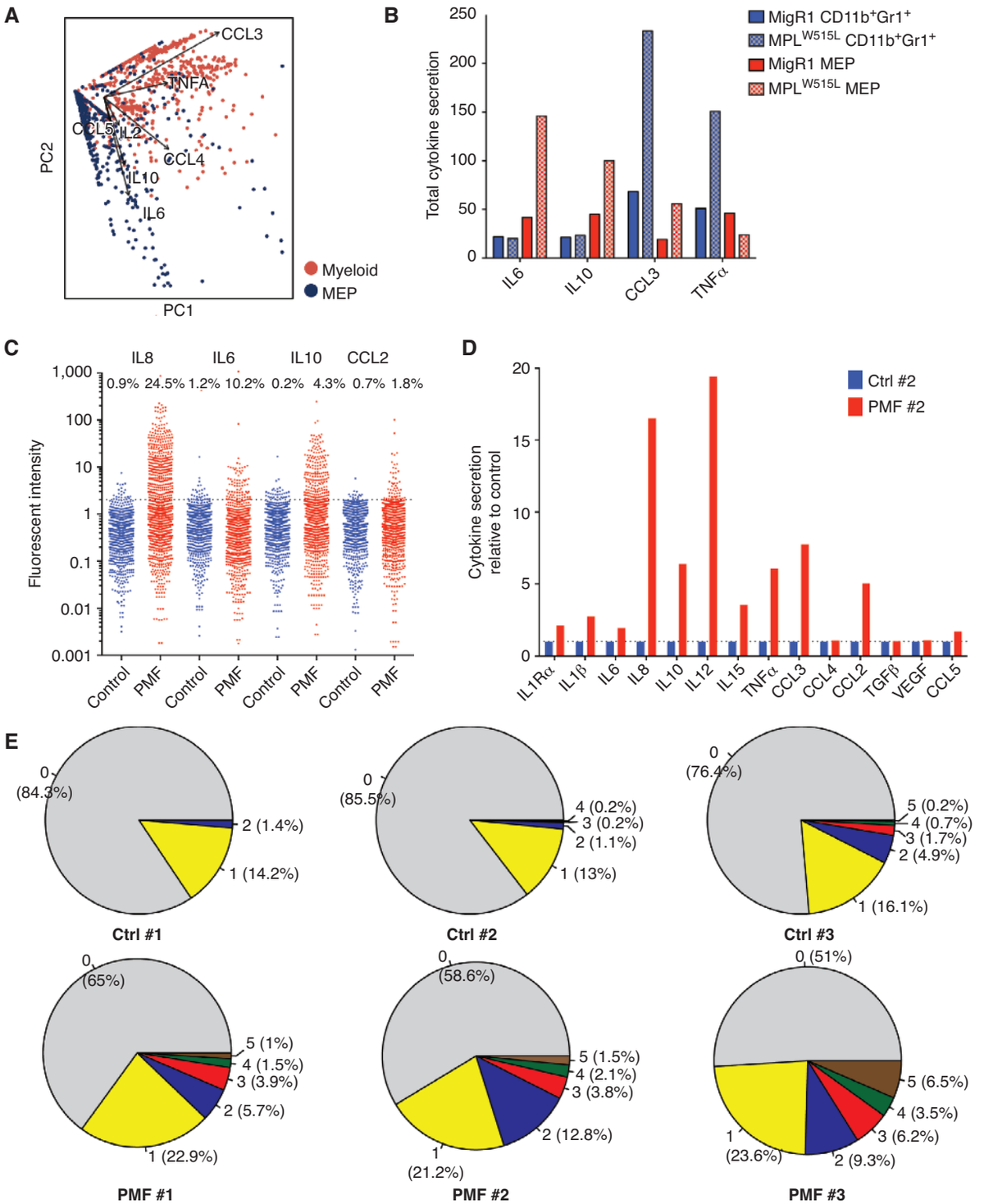

Figure 3. Pathologic secretion of multiple cytokines by myelofibrosis cells. **A,** PCA analysis of single-cell cytokine secretion data from MPL^{W515L}-expressing MEP and myeloid cells identified two principal components, largely defined by production of IL6 and IL10 (PC1 and MEP), CCL3, and TNFα (PC2, myeloid). **B,** total secretion levels (cytokine secretion fraction × average secretion intensity of cytokine secreting cells) of sorted GFP-positive cells from MPL^{W515L} mice bone marrow (MPL^{W515L}) compared with control healthy mice (MigR1) are shown. **C,** normalized fluorescent intensity for different cytokines. Numbers on top show cytokine secretion frequency. Dotted lines indicate cytokine secretion threshold. **D,** total secretion levels of human PMF granulocytes (PMF #2) relative to control cells (Ctrl #2) are shown. PMF #2: $n = 1{,}318$ analyzed cells; control granulocytes: $n = 976$ analyzed cells. **E,** pie charts depicting percentage of human PMF granulocytes (PMF) and control cells secreting different numbers of cytokines. Numbers in parentheses represent the percentage of cells secreting a given number of cytokines.

Published OnlineFirst January 8, 2015; DOI: 10.1158/2159-8290.CD-14-0736

cytokines remained elevated in IL6-deficient myelofibrosis mice, and we observed compensatory increases in IL4 and IL5 serum levels in the absence of IL6 production (Supplementary Fig. S5E and S5F). Although the specific role of other cytokines in myelofibrosis requires further investigation, these data suggest that inflammatory signaling in MPN is driven by multiple cytokines, and that inhibiting secretion or signaling of an individual cytokine cannot attenuate the cytokine-signaling loop contributing to MPN pathogenesis.

Deletion of *Stat3* Reduces Cytokine Production and Ameliorates Myelofibrosis *In Vivo*

We next aimed to investigate whether there are specific signaling pathways driving cytokine production *in vivo* in myelofibrosis. First, to better characterize oncogenic signaling pathways activated by *JAK2/MPL* alleles *in vitro* and identify potential signaling effectors, we generated isogenic cell lines expressing the most common *JAK2* and *MPL* mutations observed in patients with MPN. Notably, Ba/F3 cells expressing MPL^{W515L} or MPL^{W515L}–$JAK2^{V617F}$ showed evidence of constitutive STAT3 activation (Supplementary Fig. S6). We also observed increased STAT3 phosphorylation in splenocytes from MPL^{W515L}-diseased mice and in the bone marrow of patients with PMF (Supplementary Fig. S7). JAK inhibitor therapy reduced STAT3 phosphorylation *in vivo* (Fig. 4A).

Previous studies have shown that STAT3 signaling contributes to cytokine production in different malignant and inflammatory contexts (20); however, the role of STAT3

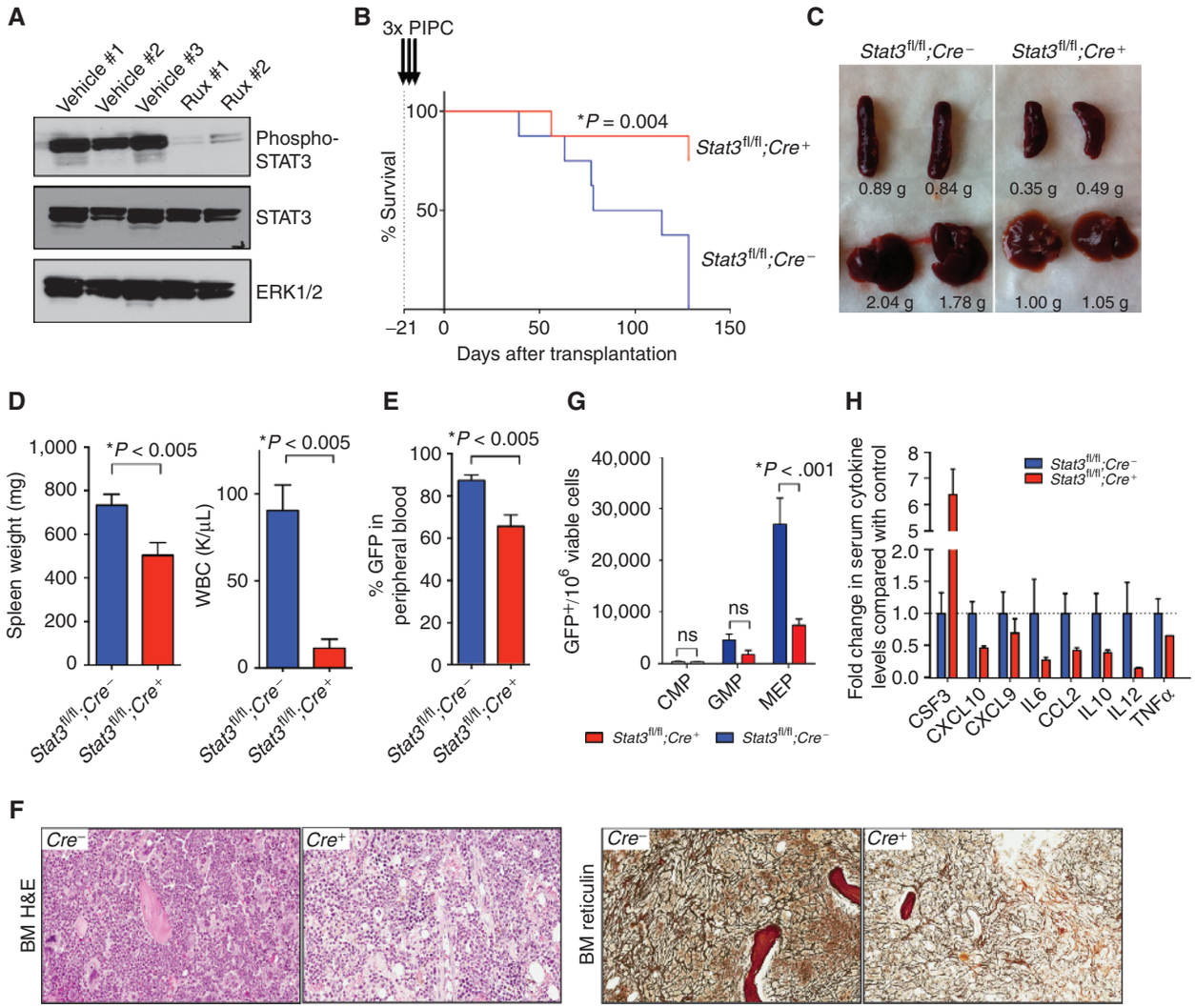

Figure 4. Deletion of *Stat3* reduces cytokine production and ameliorates myelofibrosis *in vivo*. **A,** Western blot analysis of splenocytes from vehicle/ruxolitinib (Rux)–treated MPL^{W515L}-mutant diseased mice. **B–D,** deletion of *Stat3* prolongs survival (**B**; $n = 8$) and reduces organomegaly (**C**) and leukocytosis (**D**) in the MPL^{W515L} BMT model compared with control mice. Mean ± SEM of two independent experiments. **E,** peripheral blood flow cytometric analysis. **F,** reduced bone marrow (BM) cellularity and reticulin fibrosis in the bone marrow of MPL^{W515L}-expressing $Stat3^{fl/fl}$;*Vav-Cre*$^+$ and MPL^{W515L}-expressing $Stat3^{fl/fl}$;*Vav-Cre*$^-$ mice. Representative pictures of three independent experiments; ×20 magnification. H&E, hematoxylin and eosin. **G,** number of GFP-positive MEP cells is decreased in the bone marrow of mice transplanted with MPL^{W515L}-expressing *Stat3*-deleted bone marrow compared with MPL^{W515L}-diseased controls. Mean ± SEM of two independent experiments. *Vav-Cre*$^+$: $n = 16$; *Vav-Cre*$^-$: $n = 10$. **H,** *Stat3* deletion reduces serum cytokines in MPL^{W515L}-transplanted recipient mice. *Vav-Cre*$^+$: $n = 10$; *Vav-Cre*$^-$: $n = 7$. Mean ± SEM.

Published OnlineFirst January 8, 2015; DOI: 10.1158/2159-8290.CD-14-0736

signaling in MPN inflammatory signaling and pathogenesis has not yet been elucidated. We thus performed MPL^{W515L} bone marrow transplantations using hematopoietic-specific conditional *Stat3*-knockout mice or respective littermate controls as donors (Supplementary Fig. S8). *Stat3* deletion improved survival, reduced disease severity, and reduced cytokine-mediated inflammation, similar to the effects observed with ruxolitinib therapy. *Stat3* deletion resulted in lower white blood counts, lower spleen weights, and a reduced degree of reticulin fibrosis (Fig. 4B–F and Supplementary Fig. S6), and decreased the proportion of MEP cells in spleen and bone marrow (Fig. 4G). Similar effects of *Stat3* deletion were seen with *Mx-Cre* and *Vav-Cre*, and with somatic deletion of *Stat3* after bone marrow transplantation (Supplementary Fig. S9). Most importantly, hematopoietic specific *Stat3* deletion normalized circulating cytokine levels (Fig. 4H), with similar reductions in cytokine levels as with ruxolitinib therapy. These data demonstrate that STAT3 activation is required for cytokine production in myelofibrosis, and *Stat3* deletion phenocopies the effects of ruxolitinib on cytokine production and on disease sequelae *in vivo*.

Mutant-Specific *Stat3* Deletion Does Not Reduce Inflammatory Signaling or Myelofibrosis *In Vivo*

It is currently not known if JAK inhibitors achieve clinical benefit solely from target inhibition in MPN cells, or if JAK–STAT inhibition in nonmalignant cells contributes to therapeutic efficacy. We therefore examined whether restricting *Stat3* deletion to mutant hematopoietic cells would result in similar effects as pan-hematopoietic *Stat3* deletion. We transplanted lethally irradiated CD45.1-positive recipient mice with MPL^{W515L}-positive, *Stat3*-deleted bone marrow (CD45.2-positive) along with *Stat3* wild-type support marrow (CD45.1-positive; Fig. 5A and B). In contrast to the

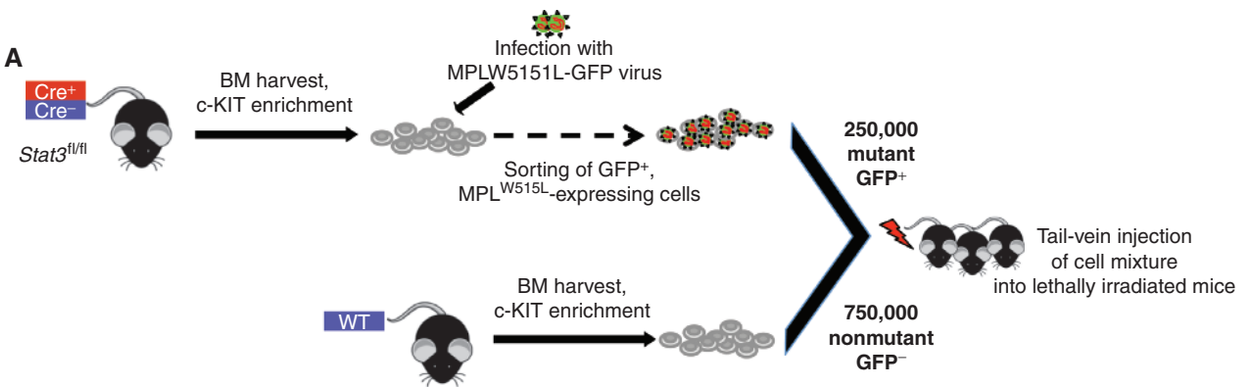

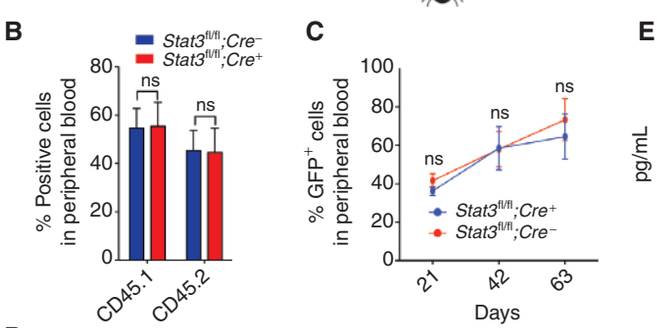

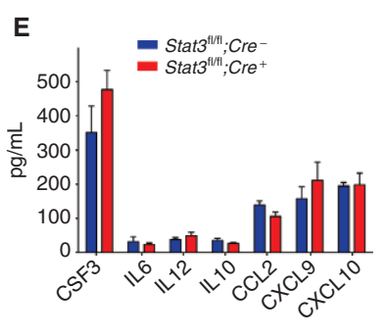

D

	Stat3$^{fl/fl}$;*vav*$^{-}$ *n* = 10	*Stat3*$^{fl/fl}$;*vav*$^{+}$ *n* = 10	*P*
WBC (K/μL)	30.02 ± 8.48	19.73 ± 5.55	ns
HCT (%)	69.08 ± 3.89	53.2 ± 5.57	<0.05
Platelets (K/μL)	901.90 ± 172.62	928.10 ± 249.57	ns
RBC	11.74 ± 0.86	10.36 ± 1.12	ns
Hb	17.59 ± 0.94	14.4 ± 1.35	ns
GFP^{+}cells PB (%)	54.18 ± 8.46	34.48 ± 10.03	ns

Figure 5. Mutant-restricted deletion of *Stat3* does not affect disease severity *in vivo*. **A,** schematic illustration of bone marrow (BM) transplantation experiments using *Stat3*-deficient mice or littermate control mice as donors. Bone marrow cells were harvested from *Stat3* knockout or wild-type (WT) control littermates, infected with MSCV-*hMPL*^{W515L}-IRES-GFP, and sorted for GFP. The 250,000 GFP-positive cells were injected with 750,000 wild-type support marrow cells into lethally irradiated, wild-type (CD45.1) recipient mice. **B,** depiction of peripheral blood chimerism of CD45.1-positive recipient mice transplanted with sorted CD45.2-positive MPL^{W515L}-expressing *Stat3*$^{fl/fl}$;*Vav-Cre*$^{\pm}$ cells and CD45.1 support (day 14 after transplantation). **C,** deletion of *Stat3* in the mutant compartment does not reduce the proportion of GFP-positive cells in the peripheral blood; *n* = 10/group of which 4 were sacrificed at day 48 for analysis. **D,** elevated cytokine levels with mutant-specific *Stat3* deletion. HCT, hematocrit; Hb, hemaglobin; PB, peripheral blood. **E,** differential blood counts of diseased mice that were transplanted with *Stat3*$^{fl/fl}$;*Cre-Vav*$^{+}$ or *Stat3*$^{fl/fl}$;*Cre-Vav*$^{-}$ MPL^{W515L} transduced cells with 500,000 wild-type support marrow. *n* = 10/group.

Published OnlineFirst January 8, 2015; DOI: 10.1158/2159-8290.CD-14-0736

significant effects seen with complete hematopoietic *Stat3* deletion, MPN-specific *Stat3* deletion did not reduce disease severity (Fig. 5C and D and Supplementary Fig. S10). Consistent with these data, MPN-specific *Stat3* deletion did not significantly attenuate cytokine production, in contrast to the effects observed with pan-hematopoietic *Stat3* deletion (Fig. 5E). These data are consistent with a requirement for STAT3 signaling in both malignant and nonmalignant hematopoietic cells in myelofibrosis.

Cytokine Production in Myelofibrosis Originates in Malignant and Nonmalignant Hematopoietic Cells

The genetic studies described above suggested that aberrant cytokine production in myelofibrosis emanates from malignant and nonmalignant hematopoietic cells. We therefore analyzed cytokine mRNA expression in sorted *MPL*^{W515L}-mutant (GFP-positive) and wild-type (GFP-negative) bone marrow cells using NanoString technology. We found that *MPL*^{W515L}-mutant myelofibrosis cells express high mRNA levels of a subset of inflammatory cytokines, including *Il6*, consistent with tumor-derived cytokine production (Fig. 6A). In contrast, we found that some cytokines, including *Ccl2* and *Tnfa*, were derived from both GFP-positive and GFP-negative populations, and other cytokines, including *Il12* and *Cxcl9*, were largely derived from nonmutant cells (Fig. 6A).

We then performed single-cell analysis of sorted mutant and wild-type subpopulations to further delineate the contribution of malignant and nonmalignant cells to cytokine production. Single-cell analysis of lineage-positive (mature) and lineage-negative [hematopoeitic stem/progenitor (HSPC)] cells revealed that GFP-positive and GFP-negative cells from mature and HSPC compartments aberrantly secrete cytokines in myelofibrosis (Fig. 6B and C). We observed an increase in cytokine secretion and in the degree of single-cell cytokine secretion heterogeneity in both GFP-positive and GFP-negative cells from stem/progenitor and differentiated cells compared with control bone marrow cells (Supplementary Fig. S11). *MPL*^{W515L}-mutant HSPCs were the largest source of IL6, whereas nonmutant mature cells were the primary source of CXCL9 (Fig. 6B). Mutant and wild-type cells both secreted TNFα, IL10, and CCL2 consistent with production by multiple populations (Fig. 6C). We observed an increase in total cytokine production and an increase in the proportion of cells which secreted multiple cytokines in GFP-positive/negative mature and GFP-positive HSPC from myelofibrosis mice (Fig. 6D and Supplementary Figs. S11 and S12). Importantly, ruxolitinib treatment normalized cytokine expression from GFP-positive and GFP-negative cell populations (Fig. 6E), demonstrating that JAK inhibition reduces cytokine production from both tumor and nontumor populations *in vivo*.

We next sought to extend our findings to *JAK2*^{V617F}-mutant MPN. We transplanted whole bone marrow of *Jak2*^{V617F}*;Vav-Cre* knockin mice (CD45.2) with CD45.1 wild-type support marrow into CD45.1-recipient mice (MPN mice). After all mice were engrafted with JAK2^{V617F}-positive disease, we performed single-cell cytokine analysis on sorted CD45.2 and CD45.1 cells to elucidate cytokine secretion in mutant and nonmutant cells (Fig. 7A). As a control, we transplanted wild-type CD45.2 bone marrow with CD45.1 support cells into CD45.1-recipient mice (control mice). Single-cell cytokine profiling revealed marked differences in cytokine secretion in bone marrow cells derived from MPN and control mice (Supplementary Fig. S13). Most importantly, this included aberrant cytokine production in CD45.2-mutant and CD45.1-nonmutant cells from MPN mice. We observed an increase in the fraction of cytokine-secreting cells and in the extent of cytokine secretion per single cell in mutant and nonmutant hematopoietic populations from *Jak2*-mutant MPN mice (Fig. 7B and C and Supplementary Fig. S14). The proportion of cells secreting at least one cytokine was significantly higher within the wild-type population (CD45.1) of myelofibrosis mice compared with the CD45.1 population of control mice (47.1% vs. 27%; $P < 0.001$; Fisher exact test; Fig. 7D). Similarly, 65% of CD45.2-positive JAK2^{V617F}-expressing cells from myelofibrosis mice secreted at least one cytokine compared with only 28.5% of control CD45.2 cells ($P < 0.001$; Fisher exact test). Furthermore, *Jak2*^{V617F}-negative CD45.1-positive and *Jak2*^{V617F}-positive CD45.2-positive bone marrow cells from myelofibrosis exhibited a marked increase in the proportion of multifunctional cells that cosecrete multiple cytokines (Fig. 7D). Quantification of the extent of heterogeneity using the Simpson diversity index showed that nonmutant CD45.1-positive and *Jak2*^{V617F}-positive, CD45.2-positive cells of diseased mice featured a significant increase in the heterogeneity of single-cell secretion (CD45.1: 0.64 vs. 0.43, CD45.2: 0.74 vs. 0.44). Consistent with these data and with our data in the MPL^{W515L} model, ruxolitinib treatment normalized cytokine expression from CD45.1-negative and CD45.2-positive cell populations in the *Jak2*^{V617F} knockin transplantation model (Supplementary Fig. S15). We next sought to investigate whether mutant and nonmutant cells in PMF could contribute to aberrant cytokine secretion. We identified a patient with PMF with a *JAK2*^{V617F}-mutant allele burden of 38%, consistent with partial involvement of the hematopoietic compartment of *JAK2*^{V617F}-mutant

Figure 6. Proinflammatory cytokines are derived from malignant and nonmalignant hematopoietic cells. **A,** NanoString mRNA cytokine expression levels in GFP-positive (GFP$^+$) and GFP-negative (GFP$^-$) cells. Normalized expression values calculated as relative change compared with GFP-negative cells. Results of one of two replicate experiments are displayed. **B,** single-cell cytokine analysis of sorted populations showing fluorescent intensity. MigR1-expressing bone marrow was used as control. Percentages of cytokine-secreting cells are shown above. Dashed line indicates normalized cytokine secretion threshold. **C,** cytokine expression of sorted GFP-positive/GFP-negative lineage-positive (LIN$^+$) and lineage-negative (LIN$^-$) cells of MPL^{W515L}-diseased mice relative to MigR1 control bone marrow. **D,** pie charts depicting percentage of sorted GFP-negative/positive lineage-positive/negative myelofibrosis cells and MigR1 control cells secreting different numbers of cytokines. Numbers in brackets represent the percentage of cells secreting a given number of cytokines. **E,** NanoString expression data (mean ± SEM) for lineage-positive GFP-positive and GFP-negative cells from vehicle/ruxolitinib-treated MPL^{W515L}-diseased mice. Data from MigR1 transplanted mice are shown as control. $n = 3$/group.

Published OnlineFirst January 8, 2015; DOI: 10.1158/2159-8290.CD-14-0736

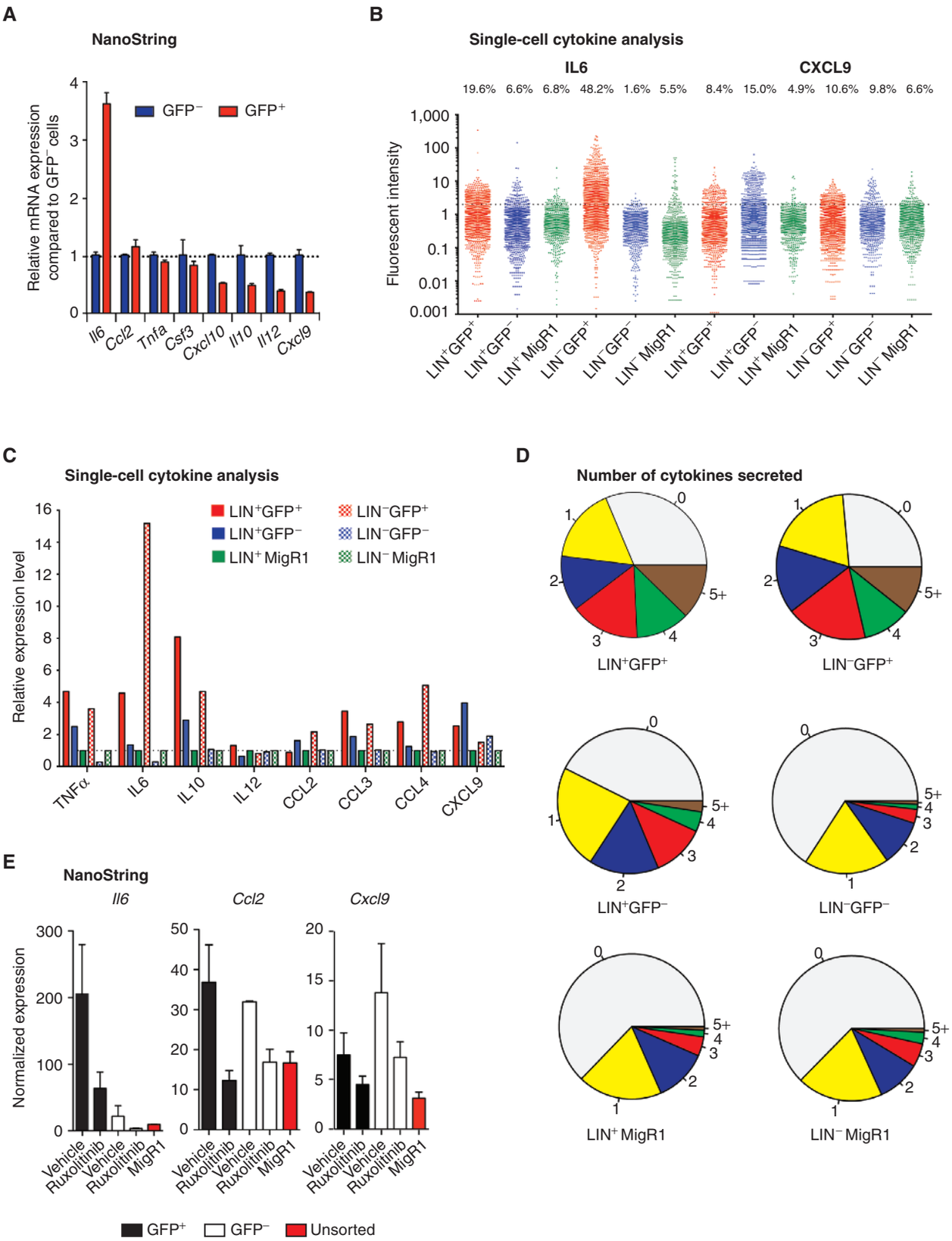

Published OnlineFirst January 8, 2015; DOI: 10.1158/2159-8290.CD-14-0736

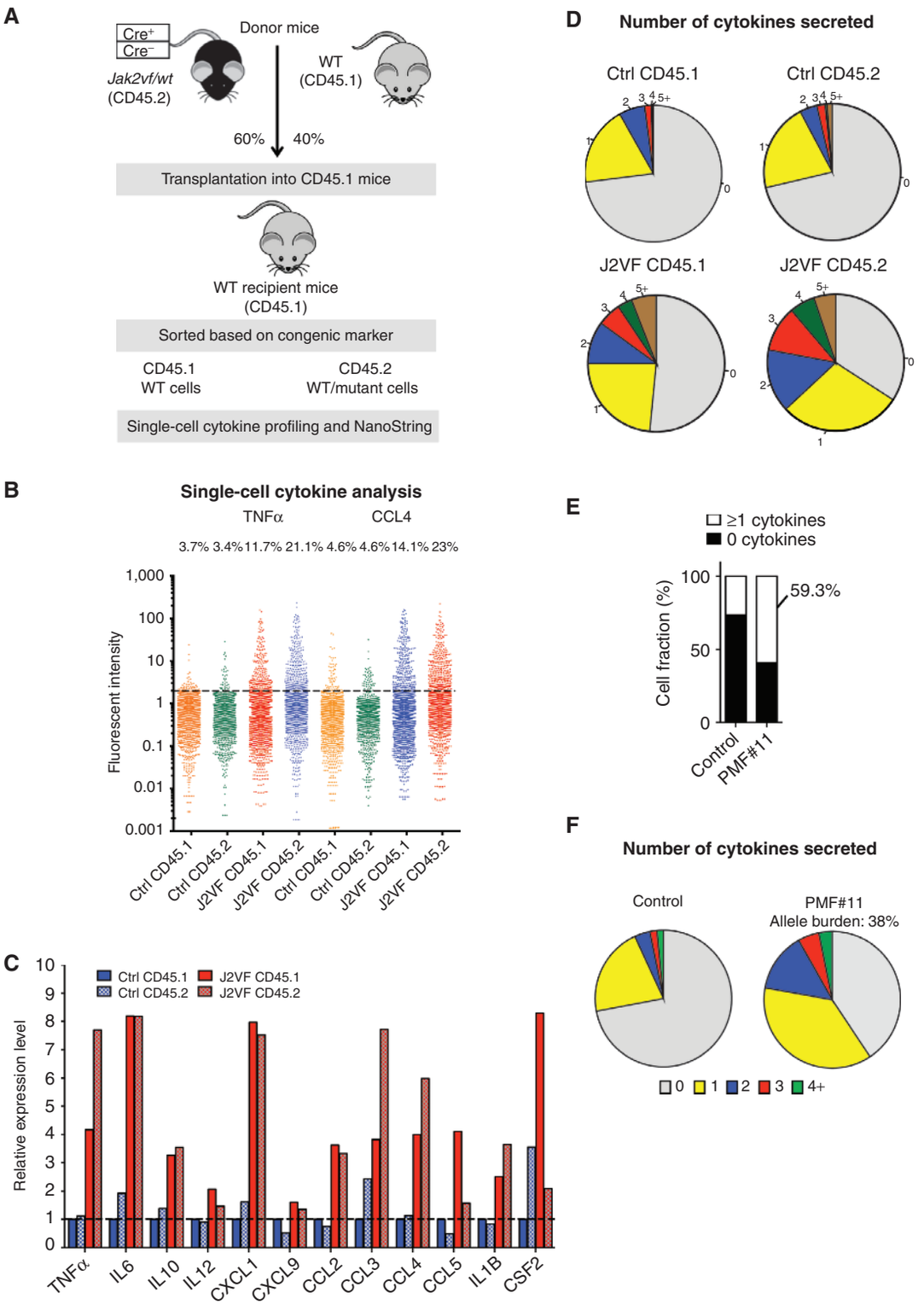

Figure 7. Aberrant cytokine production in CD45.2-mutant and CD45.1-nonmutant cells from JAK2^{V617F}-diseased mice. **A,** schematic illustration of bone marrow transplantation experiments using *Jak2*^{V617F};*Vav-Cre* knockin mice (CD45.2) as donors. **B,** single-cell analysis of sorted mutant (CD45.2) and nonmutant (CD45.1) populations from *Jak2*^{V617F}-mutant diseased mice (J2VF) and transplanted healthy controls (Ctrl). Percentages of cytokine secreting cells are shown above. **C,** cytokine expression levels of sorted CD45.1-positive and CD45.1-negative myelofibrosis and *Vav-Cre*–negative control cells relative to CD45.1 control cells. **D,** pie charts displaying the percentage of sorted mutant (CD45.2) and nonmutant (CD45.1) secreting different numbers of cytokines (0, 1, 2, 3, 4, 5+). **E,** cytokine secretion data showing that 59.3% of human PMF cells (patient PMF#11, allele burden: 38%) secrete at least one cytokine. **F,** pie charts depicting the percentage of human PMF cells and control cells secreting different numbers of cytokines (0, 1, 2, 3, 4+).

Published OnlineFirst January 8, 2015; DOI: 10.1158/2159-8290.CD-14-0736

cells (Supplementary Table S2). Notably, in this patient we found that 59% of the hematopoietic cells secreted one or more cytokines from our measurement (Fig. 7E). Moreover, the frequency of multifunctional cells secreting two or more cytokines was significantly elevated in the patient (Fig. 7F). The proportion of cytokine-secreting cells was greater than expected on the basis of *JAK2*^{V617F}-mutant allele burden, suggesting that in this patient, a subset of *JAK2*^{V617F} wild-type has to contribute to cytokine production. Taken together, these data illustrate the heterogeneity of aberrant cytokine secretion in MPN models and patients, and that aberrant inflammatory signaling from more than one population contributes to MPN pathogenesis and therapeutic response.

DISCUSSION

Although MPNs present as chronic myeloid malignancies, the quality of life and overall survival of patients with PMF is more similar to advanced malignancies, including metastatic epithelial tumors. Patients with PMF have markedly elevated levels of proinflammatory cytokines, which are thought to contribute to PMF-associated symptoms and sequelae (12, 13). Clinical data show that JAK inhibition reduces constitutional symptoms and splenomegaly in patients with PMF and post–PV/ET myelofibrosis, concurrent with a reduction in circulating cytokine levels (13). Although the prognostic value of circulating cytokine levels in myelofibrosis has been previously demonstrated (12), the mechanisms that govern aberrant cytokine production in myelofibrosis and the source of aberrant cytokines in myelofibrosis have not previously been demonstrated. Here, we show that JAK–STAT activation in malignant and nonmalignant cells contributes to myelofibrosis pathogenesis, and that cytokine production by both populations is an important feature of myelofibrosis.

In this study, we demonstrate that JAK1/2 inhibition leads to a rapid, potent reduction in serum cytokine levels, consistent with the rapid clinical benefits seen with JAK inhibitor therapy, and demonstrate that this is a direct effect of JAK kinase inhibition on cytokine production. Single-cell cytokine analysis showed that hematopoietic cells from myelofibrosis models and patients with PMF aberrantly secrete a spectrum of inflammatory cytokines. We performed multiplex, highly sensitive measurements of cytokine secretion from over a thousand captured, viable single cells. The results demonstrated that hematopoietic cells in myelofibrosis show significant upregulation of a spectrum of proinflammatory cytokines, elevation of cellular heterogeneity in cytokine secretion, and increased multifunctional cytokine production, which are not observed in normal hematopoietic cells. Our data on a specific lineage, myeloid, demonstrated that both mature and progenitor myeloid cells contribute to increased cytokine production, and more interestingly that they show distinct cytokine profiles, suggesting their different roles in myelofibrosis pathogenesis. Future studies will delineate the role of additional cytokines in inflammatory signaling in MPN, and use single-cell profiling to analyze nonhematopoietic cell types and previously unexplored hematopoietic lineages, such as lymphoid cells and purified stem cells, in MPN models/patient samples and in other malignancies to determine whether multifunctional cytokine secretion is observed in other malignant contexts.

Many studies have identified *JAK2* mutations in patients with MPN and in other malignancies, and several known JAK2 signaling mediators have been linked to MPN disease manifestation and progression (21–23); however, the role of STAT3 signaling in MPN pathogenesis and in inflammatory signaling in myeloid malignancies has not been previously delineated. STAT3 represents a key link between cancer and inflammation, and as such provides an ideal candidate signaling effector driving cytokine production *in vivo*. In this study, we demonstrate a critical role for STAT3 in inflammatory cytokine production in myelofibrosis. Pan-hematopoietic *Stat3* deletion improved survival, reduced disease severity, and reduced cytokine secretion, with similar efficacy as observed with ruxolitinib therapy. In contrast, restricting loss of *Stat3* to the malignant clone did not reduce disease severity or cytokine production, demonstrating that STAT3 signaling must be inhibited in malignant and nonmalignant cells to achieve clinical efficacy. Consistent with these findings, we discovered that malignant and nonmalignant cells aberrantly secrete inflammatory cytokines and that JAK inhibition reduces cytokine production from both populations. Our results demonstrate that JAK–STAT3-mediated cytokine production from malignant and nonmalignant cells contributes to MPN pathogenesis and that JAK inhibition in both populations is required for therapeutic efficacy. These data reveal an important, unexpected mechanism of action of JAK inhibition in MPN, such that the target must be inhibited in tumor and nontumor cells to achieve clinical benefit.

Recent studies in MPN models and in other hematologic malignancies have shown that additional, nonhematopoietic populations can influence malignant transformation, including nestin-positive stromal cells, osteoblasts, and other cell types in the hematopoietic niche (24–26). The role of cytokine secretion from these additional populations, particularly at single-cell resolution, has not been explored to date. We believe that single-cell cytokine profiling can be used to elucidate the specific role of different niche populations in normal and malignant hematopoiesis and to assess the impact of JAK inhibitor therapy on the nonhematopoietic microenvironment in model systems and in primary patient samples, which should be the subject of subsequent investigations into cytokine secretion in different malignant states.

Taken together, our data underscore the critical role of aberrant cytokine signaling mediated by STAT3 activation in MPN pathogenesis. Most importantly, our studies support the notion that JAK kinase inhibition in malignant and nonmalignant cells is required to achieve clinical efficacy in myelofibrosis. Recent data have suggested that ruxolitinib improves overall survival in patients with pancreatic cancer with evidence of systemic inflammation. As such, inhibition of cytokine signaling in malignant and nonmalignant cells might offer clinical benefit in other malignancies characterized by aberrant inflammatory signaling. We hypothesize that

Published OnlineFirst January 8, 2015; DOI: 10.1158/2159-8290.CD-14-0736

JAK inhibition may have a broader role in cancer therapy, and that this therapeutic approach may improve outcomes for patients with malignancies characterized by systemic inflammation.

METHODS

Patient Material

Patient studies were conducted in accordance with the Declaration of Helsinki. Primary patient samples were collected from patients with myelofibrosis and control healthy donors under Memorial Sloan Kettering Cancer Center (MSKCC; New York, NY) Institutional Review Board Protocol 09-141. Ficoll technique was applied to isolate granulocytes from the peripheral blood of patients with myelofibrosis and healthy control individuals. *JAK2* allele burden for patients with myelofibrosis was calculated using targeted sequencing approaches (RainDance, MiSeq).

Reagents and Transgenic Mice

Ruxolitinib was provided by Incyte/Novartis and formulated for administration by oral gavage as previously described (27). Conditional *Stat3* knockout, *Jak2*^{V617F} knockin, and germline *Il6* knockout mice have been described previously (15, 28). Floxed mice were crossed to the interferon-responsive *Mx-Cre* and *Vav-Cre* deleter lines. Congenic mice (CD45.1) used as recipients in transplant studies were purchased from The Jackson Laboratory. Antibodies used for Western blotting included phosphorylated and total JAK2, STAT3, STAT5, and MAPK (Cell Signaling Technology). Mutant (GFP-positive) and wild-type (GFP-negative) populations were separated by FACS using GFP and/or specific cell-surface marker: phycoerythrin (PE)-conjugated CD11b, allophycocyanin (APC)-conjugated Gr1, TER119 (APC-CY7), CD71 (PE-CY7), PE-conjugated CD117, Pacific Blue (PacBlue)–conjugated CD16/CD32, phycoerythrin-Cy7 (PeCy7)–conjugated Sca-1, and APC-conjugated CD34. All plasmids used in this study have been previously described (29). Lineage-positive (LIN$^+$) and lineage-negative (LIN$^-$) subpopulations were separated using a panel of APC-CY7–conjugated antibodies that recognize all mature hematopoietic lineages (CD4, CD19, CD11b, Gr1, TER119, CD3, B220, and NK1.1).

Bone Marrow Transplantation Model

All animal experiments were performed in accordance with our MSKCC Institutional Animal Care and Use Committee–approved animal protocol. Animal care was in strict compliance with institutional guidelines established by the MSKCC, the Guide for the Care and Use of Laboratory Animals (National Academy of Sciences, 1996), and the Association for Assessment and Accreditation of Laboratory Animal Care International. MPL^{W515L} bone marrow transplantation experiments were performed as described previously (14). Briefly, prestimulated c-KIT enriched bone marrow cells were subjected to two rounds of cosedimentation with viral supernatant containing MSCV-*hMpl*^{W515L}-IRES-GFP or empty MSCV-IRES-GFP control vector. A total of 1×10^6 cells (~25%–40% GFP-positive, MPL-expressing cells) were injected into the tail veins of lethally irradiated syngeneic mice. For secondary *Jak2*^{V617F};*Vav-Cre* bone marrow transplantations, 5×10^6 bone marrow cells harvested from sick *Jak2*^{V617F} knockin mice were injected into the tail veins of 8-week-old syngeneic mice (15). Engrafted mice were monitored daily for signs of illness, and nonlethal bleeds were performed biweekly to follow up disease progression. Mice showing signs of being moribund, having more than 10% weight loss, or having palpable splenomegaly extending across the midline were sacrificed. Spleens were removed and weighed, and single-cell suspensions were prepared for subsequent cell staining and fractionation, Western blot analysis, or histopathologic analysis. Peripheral blood chimerism was routinely determined 14 days after bone marrow transplantation. *Stat3* excision was confirmed by Western blot analysis and quantitative real-time PCR analysis on red cell lysed peripheral blood samples.

Inhibitor Experiments

At first signs of disease, mice were randomized to begin 14 or 21 days of treatment with the JAK1/2 inhibitor ruxolitinib [90 mg/kg (Balb/c, *Mpl*^{W515L}) or 60 mg/kg (C57/BL6, secondary *Jak2*^{V617F} recipient mice), *p.o.*, twice a day] or vehicle followed by measurement of plasma cytokine levels. Mice were ranked on the basis of baseline WBC count and assigned to treatment groups to achieve congruent WBC profiles. Serum was collected 4 hours after last drug administration. For kinetic studies, mice assigned for short-term drug treatment received only three doses, which were administered simultaneously with the last doses of the long-term treatment arm.

Luminex Technology

Luminex assays were carried out using the FlexMAP 3D multiplexing platform (Luminex xMAP system). Plasma levels of 32 cytokines were measured simultaneously using the Millipore Mouse Cytokine 32-plex kit. Serum samples were prepared following manufacturer's instructions. xPONENT (Luminex) and Milliplex Analyst Software (Millipore) was applied to convert mean fluorescent intensity values into molecular concentrations by the use of a standard curve (5-parameter logistic fitting method).

Histopathologic Analysis

Femur and spleen samples were fixed in 4% paraformaldehyde overnight and then embedded in paraffin as previously described (30). Paraffin sections were cut on a rotary microtome (3-μm; Mikrom International AG), spread in a 45°C water bath, mounted on microscope slides (Thermo Scientific), and air-dried in an oven at 37°C overnight. After drying, tissue section slides were processed either automatically for hematoxylin and eosin (H&E) staining (COT20 stainer, Medite) or manually for reticulum staining with silver impregnation method kit (Bio-Optica). Slides were scanned with Scanscope XT slide scanner (Aperio). Pictures were taken at a 20× (H&E and reticulin) magnification by using Imascope viewer (Aperio). For the expression analysis of IL8 and phospho-STAT3, 5-μm unstained sections from cases of bone marrow samples were stained on the Ventana Discovery XT per the manufacturer's instructions. The following antibodies were used: goat anti-IL8 antibody from R&D Systems (1:40 dilution), monoclonal rabbit anti–phospho-STAT3 antibody from Cell Signaling Technology (1:50 dilution). Photomicrographs were taken using an Olympus BX41 with DP20 software.

Single-Cell Cytokine Secretion Assay

A high-density antibody barcode was created using a microchannel-guided flow patterning technique as previously described (16, 17). A polydimethylsiloxane microchip with 20 microfluidic channels for flow patterning was fabricated using a soft lithography technique. After the microchip was bonded with a poly-L-lysine glass slide, the capture antibody for each cytokine was injected into a microfluidic channel and flowed through the chip via air pressure (1.8 psi, 12 hours). Antibodies were then immobilized on the glass slide to form the antibody barcode. The subnanoliter microchamber array for single-cell capture is a one-layer polydimethylsiloxane slab fabricated using a soft-lithography method and contains 7,700

Published OnlineFirst January 8, 2015; DOI: 10.1158/2159-8290.CD-14-0736

microchambers (16, 31). A single-cell suspension of bone marrow cells was prepared in RPMI-1640 supplemented with 20% FBS, IL3, SCF, and IL6 at a density of 4×10^5 cells/mL. After blocking with 3% BSA/PBS (2 hours), 200 μL of the single-cell suspension was pipetted onto the chip and allowed to settle (5 minutes). Normally approximately 25% of the microchambers contained single cells based on the Poisson distribution (16). The antibody barcode glass slide was then put on top of the microchambers. Assembled microchamber arrays were then imaged (Nikon Eclipse Ti) to determine the number of cells in each microchamber by using a custom-made image-processing algorithm. After incubation (24 hours, 37°C in 5% CO_2), the cytokine signals from antibody barcode chips were developed via an immuno-sandwich ELISA assay. The slide was scanned with GenePix 4200A (Axon) microarray scanner to collect fluorescent signals. All fluorescent scanned images were processed with GenePix software and Excel macro to acquire average fluorescent signals from each microchamber for all bars in each antibody barcode set, and the fluorescent signals were matched with the number of cells. Single-cell data were gated on the basis of the background signals to distinguish between cytokine producers and nonproducers. The data were further transformed and normalized to perform multidimensional data analysis as previously described (17, 32–34).

Data Processing and Analysis of Single-Cell Cytokine Assays

For all single-cell secretomic analysis, our custom-built algorithms in Excel, MATLAB, and R-packages were used to process, analyze, and visualize the single-cell cytokine profiles. Briefly, the predetermined cell numbers of the microchambers were matched with fluorescence intensity values for each measured protein from corresponding microchambers. The background signals from all zero-cell (empty) microchambers were used to determine the gate to detect cytokine-producing cells and nonproducers. The gating threshold was calculated by (average intensity of all empty microchambers for a given cytokine) + 2 × (standard deviation of all empty microchambers for a given cytokine) (34). Any cells with fluorescence intensity of a specific cytokine below the gating threshold were considered nonproducers, and their cytokine intensity values were converted to 0. Any cells with fluorescence intensity above the gating threshold were considered cytokine-producers and given the cytokine intensity value of (the measured fluorescence intensity − the average fluorescence intensity of all zero-cell microchambers for a given cytokine). The gated and background-subtracted cytokine intensity values were log-transformed. To eliminate variability in detection sensitivity and profile the secretion of all assayed proteins, each protein was normalized by the average intensity and the standard deviation. The number of all cells above the gates and the sum of fluorescence intensity of a given cytokine were measured to calculate the frequency of cytokine producers and the average cytokine secretion per single cell. For the single-cell analysis of unsorted, whole bone marrow compartment, the data were processed without log transformation. By not conducting log transformation, which significantly suppresses the data range, we could distinguish smaller subsets with unique cytokine profiles from the more heterogeneous and larger unsorted bone marrow cell population. Our statistical analysis and graphical representations of the single-cell secretomic profiles are based on the methods routinely used to analyze large-scale high-dimensional datasets from numerous cell subsets (17, 32–34).

Principal Component, Mutual Exclusivity, and Statistical Analysis

All analyses were performed in R. The PCA was performed using the prcomp R function and visualized with the ggplot2 package. The first two principal components explained 60.1% of the variance. PC3 and PC4 (cumulative proportion of variance 78%) were, similar to PC1 and PC2, mainly defined by secretion of TNFα, CCL3, CCL4, CXCL1, and CCL5 (Supplementary Fig. S1A). Because PC3 to PC4 covered essentially the same cytokines as PC1 and PC2, we focused on the visualization of the first two PCs. PC5 (83%) was dominated by IL10 secretion. We next tested whether two cytokines were less (mutual exclusivity) or more frequently cosecreted than expected by chance. To this end, we created for each pair of cytokines a 2 × 2 contingency table (secreted only in cytokine A; only in B; in both A and B; in neither A nor B) and obtained a *P* value with the Fisher exact test. *P* values were adjusted for multiple testing using the Benjamini–Hochberg correction and a false discovery rate (FDR) < 0.05 was considered significant. FDRs were visualized in a heat map, with pairs of cytokines displaying significant cosecretion colored in red, and mutually exclusive pairs in light yellow. Pairs with cosecretion patterns not significantly different from randomly expected patterns were shown in gray. We further tested whether pairs of cytokines are more or less frequently cosecreted in myelofibrosis mice compared with control mice. We again used a Fisher exact test to obtain *P* values for the corresponding 2 × 2 contingency table (number of cosecreted cells in myelofibrosis, number of non-cosecreted cells in myelofibrosis, number of cosecreted cells in control mice, number of non-cosecreted cells in control mice). Only cells with at least two secreted cytokines were considered in this mutual exclusivity analysis.

Statistical Analysis

The Student *t* test was used to compare the mean of two groups. Normality tests were used to test the assumption of a normal distribution. Graphs represent mean values ± SEM. Kaplan–Meier survival analysis and the log-rank test were used to compare survival outcomes between the two groups.

Disclosure of Potential Conflicts of Interest

M. Riester is a full-time employee of Novartis. J. Bromberg reports receiving a commercial research grant from AstraZeneca. M. Murakami is an investigator at Novartis and has ownership interest (including patents) in the same. R. Fan has ownership interest (including patents) in IsoPlexis. R.L. Levine reports receiving a commercial research grant from Incyte. No potential conflicts of interest were disclosed by the other authors.

Authors' Contributions

Conception and design: M. Kleppe, R.L. Levine
Development of methodology: M. Kleppe, M. Kwak, S. Marubayashi, V. Romanet, R. Fan
Acquisition of data (provided animals, acquired and managed patients, provided facilities, etc.): M. Kleppe, M. Kwak, P. Koppikar, M. Keller, L. Bastian, N. Bhagwat, E. Papalexi, O. Abdel-Wahab, R. Rampal, S. Marubayashi, J.J. Chen, J. Bromberg, J. Teruya-Feldstein
Analysis and interpretation of data (e.g., statistical analysis, biostatistics, computational analysis): M. Kleppe, M. Kwak, P. Koppikar, M. Riester, L. Bastian, T. Hricik, O. Abdel-Wahab, J.J. Chen, J.S. Fridman, M. Murakami, F. Michor, R. Fan, R.L. Levine
Writing, review, and/or revision of the manuscript: M. Kleppe, M. Kwak, M. Riester, M. Keller, O. Abdel-Wahab, S. Marubayashi, J.S. Fridman, J. Teruya-Feldstein, M. Murakami, T. Radimerski, F. Michor, R. Fan, R.L. Levine
Administrative, technical, or material support (i.e., reporting or organizing data, constructing databases): M. Kleppe, M. Kwak, M. Keller, T. Hricik, A.S. McKenney, J.J. Chen, J.S. Fridman
Study supervision: F. Michor, R. Fan, R.L. Levine

Acknowledgments

The authors thank the members of the Levine and Fan laboratories, Neal Rosen, and Scott Armstrong for helpful comments and

Published OnlineFirst January 8, 2015; DOI: 10.1158/2159-8290.CD-14-0736

discussion. The authors also thank Benjamin L. Ebert (Harvard Medical School, Boston, MA) and Ann Mullally (Harvard Medical School) for providing *Jak2*^{V617F} knockin mice. The authors are grateful to the MSK Kravis Center for Molecular Oncology/Geoffrey Beene Core for their assistance with NanoString and targeted sequencing analysis and Irina Linkov (IHC Pathology Core) and Janine Pichardo for technical assistance with pathologic experiments. The authors also acknowledge support from the Yale Institute for Nanoscience and Quantum Engineering (YINQE) and the Yale Nanofabrication Center for allowing use of their microfabrication facilities.

Grant Support

This work was supported by the Dana-Farber Cancer Institute's Physical Sciences Oncology Center (U54CA143798-01), to R.L. Levine, R. Fan, M. Riester, and F. Michor; NCI 1R01CA151949-01 to R.L. Levine; and NCI 1R01CA138234-01 to F. Michor and R.L. Levine, and partly by NIDDK 1U01DK104331-01 to R. Fan and R.L. Levine. M. Kleppe is a fellow of the Leukemia and Lymphoma Society and was previously supported by an EMBO Long-Term Fellowship. A.S. McKenney was supported by a Medical Scientist Training Program grant from the National Institute of General Medical Sciences of the NIH under award number T32GM007739 to the Weill Cornell/Rockefeller/Sloan Kettering Tri-Institutional MD–PhD Program.

The costs of publication of this article were defrayed in part by the payment of page charges. This article must therefore be hereby marked *advertisement* in accordance with 18 U.S.C. Section 1734 solely to indicate this fact.

Received July 11, 2014; revised December 23, 2014; accepted December 30, 2014; published OnlineFirst January 8, 2015.

REFERENCES

1. Tefferi A, Vardiman JW. Myelodysplastic syndromes. N Engl J Med 2009;361:1872–85.
2. Tam CS, Nussenzveig RM, Popat U, Bueso-Ramos CE, Thomas DA, Cortes JA, et al. The natural history and treatment outcome of blast phase BCR-ABL- myeloproliferative neoplasms. Blood 2008;112:1628–37.
3. Delhommeau F, Jeziorowska D, Marzac C, Casadevall N. Molecular aspects of myeloproliferative neoplasms. Int J Hematol 2010;91:165–73.
4. Baxter EJ, Scott LM, Campbell PJ, East C, Fourouclas N, Swanton S, et al. Acquired mutation of the tyrosine kinase JAK2 in human myeloproliferative disorders. Lancet 2005;365:1054–61.
5. Kralovics R, Passamonti F, Buser AS, Teo SS, Tiedt R, Passweg JR, et al. A gain-of-function mutation of JAK2 in myeloproliferative disorders. N Engl J Med 2005;352:1779–90.
6. Levine RL, Wadleigh M, Cools J, Ebert BL, Wernig G, Huntly BJ, et al. Activating mutation in the tyrosine kinase JAK2 in polycythemia vera, essential thrombocythemia, and myeloid metaplasia with myelofibrosis. Cancer Cell 2005;7:387–97.
7. James C, Ugo V, LeCouedic JP, Staerk J, Delhommeau F, Lacout C, et al. A unique clonal JAK2 mutation leading to constitutive signalling causes polycythaemia vera. Nature 2005;434:1144–8.
8. Klampfl T, Gisslinger H, Harutyunyan AS, Nivarthi H, Rumi E, Milosevic JD, et al. Somatic mutations of calreticulin in myeloproliferative neoplasms. N Engl J Med 2013;369:2379–90.
9. Nangalia J, Massie CE, Baxter EJ, Nice FL, Gundem G, Wedge DC, et al. Somatic CALR mutations in myeloproliferative neoplasms with nonmutated JAK2. N Engl J Med 2013;369:2391–405.
10. Tefferi A. Molecular drug targets in myeloproliferative neoplasms: mutant ABL1, JAK2, MPL, KIT, PDGFRA, PDGFRB and FGFR1. J Cell Mol Med 2009;13:215–37.
11. Quintas-Cardama A, Kantarjian H, Cortes J, Verstovsek S. Janus kinase inhibitors for the treatment of myeloproliferative neoplasias and beyond. Nat Rev Drug Discov 2011;10:127–40.
12. Tefferi A, Vaidya R, Caramazza D, Finke C, Lasho T, Pardanani A. Circulating interleukin (IL)-8, IL-2R, IL-12, and IL-15 levels are independently prognostic in primary myelofibrosis: a comprehensive cytokine profiling study. J Clin Oncol 2011;29:1356–63.
13. Verstovsek S, Kantarjian H, Mesa RA, Pardanani AD, Cortes-Franco J, Thomas DA, et al. Safety and efficacy of INCB018424, a JAK1 and JAK2 inhibitor, in myelofibrosis. N Engl J Med 2010;363:1117–27.
14. Pikman Y, Lee BH, Mercher T, McDowell E, Ebert BL, Gozo M, et al. MPLW515L is a novel somatic activating mutation in myelofibrosis with myeloid metaplasia. PLoS Med 2006;3:e270.
15. Mullally A, Lane SW, Ball B, Megerdichian C, Okabe R, Al-Shahrour F, et al. Physiological Jak2V617F expression causes a lethal myeloproliferative neoplasm with differential effects on hematopoietic stem and progenitor cells. Cancer Cell 2010;17:584–96.
16. Lu Y, Chen JJ, Mu L, Xue Q, Wu Y, Wu PH, et al. High-throughput secretomic analysis of single cells to assess functional cellular heterogeneity. Anal Chem 2013;85:2548–56.
17. Ma C, Fan R, Ahmad H, Shi Q, Comin-Anduix B, Chodon T, et al. A clinical microchip for evaluation of single immune cells reveals high functional heterogeneity in phenotypically similar T cells. Nat Med 2011;17:738–43.
18. Fan R, Vermesh O, Srivastava A, Yen BK, Qin L, Ahmad H, et al. Integrated barcode chips for rapid, multiplexed analysis of proteins in microliter quantities of blood. Nat Biotechnol 2008;26:1373–8.
19. Schepers K, Pietras EM, Reynaud D, Flach J, Binnewies M, Garg T, et al. Myeloproliferative neoplasia remodels the endosteal bone marrow niche into a self-reinforcing leukemic niche. Cell Stem Cell 2013;13:285–99.
20. Yu H, Pardoll D, Jove R. STATs in cancer inflammation and immunity: a leading role for STAT3. Nat Rev Cancer 2009;9:798–809.
21. Walz C, Ahmed W, Lazarides K, Betancur M, Patel N, Hennighausen L, et al. Essential role for Stat5a/b in myeloproliferative neoplasms induced by BCR-ABL1 and JAK2(V617F) in mice. Blood 2012;119:3550–60.
22. Yan D, Hutchison RE, Mohi G. Critical requirement for Stat5 in a mouse model of polycythemia vera. Blood 2012;119:3539–49.
23. Kleppe M, Levine RL. New pieces of a puzzle: the current biological picture of MPN. Biochim Biophys Acta 2012;1826:415–22.
24. Arranz L, Sanchez-Aguilera A, Martin-Perez D, Isern J, Langa X, Tzankov A, et al. Neuropathy of haematopoietic stem cell niche is essential for myeloproliferative neoplasms. Nature 2014;512:78–81.
25. Reynaud D, Pietras E, Barry-Holson K, Mir A, Binnewies M, Jeanne M, et al. IL-6 controls leukemic multipotent progenitor cell fate and contributes to chronic myelogenous leukemia development. Cancer Cell 2011;20:661–73.
26. Hanoun M, Zhang D, Mizoguchi T, Pinho S, Pierce H, Kunisaki Y, et al. Acute myelogenous leukemia-induced sympathetic neuropathy promotes malignancy in an altered hematopoietic stem cell niche. Cell Stem Cell 2014;15:365–75.
27. Quintas-Cardama A, Vaddi K, Liu P, Manshouri T, Li J, Scherle PA, et al. Preclinical characterization of the selective JAK1/2 inhibitor INCB018424: therapeutic implications for the treatment of myeloproliferative neoplasms. Blood 2010;115:3109–17.
28. Takeda K, Kaisho T, Yoshida N, Takeda J, Kishimoto T, Akira S. Stat3 activation is responsible for IL-6-dependent T cell proliferation through preventing apoptosis: generation and characterization of T cell-specific Stat3-deficient mice. J Immunol 1998;161:4652–60.
29. Wernig G, Gonneville JR, Crowley BJ, Rodrigues MS, Reddy MM, Hudon HE, et al. The Jak2V617F oncogene associated with myeloproliferative diseases requires a functional FERM domain for transformation and for expression of the Myc and Pim proto-oncogenes. Blood 2008;111:3751–9.
30. Koppikar P, Abdel-Wahab O, Hedvat C, Marubayashi S, Patel J, Goel A, et al. Efficacy of the JAK2 inhibitor INCB16562 in a murine model

Published OnlineFirst January 8, 2015; DOI: 10.1158/2159-8290.CD-14-0736

of MPLW515L-induced thrombocytosis and myelofibrosis. Blood 2010;115:2919–27.
31. Unger MA, Chou HP, Thorsen T, Scherer A, Quake SR. Monolithic microfabricated valves and pumps by multilayer soft lithography. Science 2000;288:113–6.
32. Bodenmiller B, Zunder ER, Finck R, Chen TJ, Savig ES, Bruggner RV, et al. Multiplexed mass cytometry profiling of cellular states perturbed by small-molecule regulators. Nat Biotechnol 2012;30:858–67.
33. Qiu P, Simonds EF, Bendall SC, Gibbs KD Jr, Bruggner RV, Linderman MD, et al. Extracting a cellular hierarchy from high-dimensional cytometry data with SPADE. Nat Biotechnol 2011;29:886–91.
34. Zhao JL, Ma C, O'Connell RM, Mehta A, DiLoreto R, Heath JR, et al. Conversion of danger signals into cytokine signals by hematopoietic stem and progenitor cells for regulation of stress-induced hematopoiesis. Cell Stem Cell 2014;14:445–59.

Published OnlineFirst January 8, 2015; DOI: 10.1158/2159-8290.CD-14-0736

AACR American Association for Cancer Research

CANCER DISCOVERY

JAK–STAT Pathway Activation in Malignant and Nonmalignant Cells Contributes to MPN Pathogenesis and Therapeutic Response

Maria Kleppe, Minsuk Kwak, Priya Koppikar, et al.

Cancer Discovery 2015;5:316-331. Published OnlineFirst January 8, 2015.